JOURNAL OF MATERIALS SCIENCE 32 (1997) 5927–5944

Assessment of melt cleanliness in A356.2 aluminium casting alloy using the porous disc filtration apparatus technique

Part II *Inclusion analysis*

L. LIU, F. H. SAMUEL
Département des Sciences Appliquées, Université du Québec à Chicoutimi Chicoutimi, Québec, Canada G7H 2B1

The data obtained on inclusion types and concentrations has been analysed in the present part in terms of their effect on filtration time and fluidity (measured by the length of solidified metal in quartz tubes). The dross, i.e., the oxide layer that formed on the surface of the molten metal, was carefully collected and its mass determined; then it was examined in a scanning electron microscope equipped with an energy-dispersive X-ray system. The results show that inclusions are not the only parameter to be considered. More importantly, it is Al_2O_3 (films or particles), which seems to be the deciding factor. It is found, however, that it is quite difficult to separate the individual role of each parameter using the porous disc filtration apparatus (PoDFA) technique, i.e., sampling, without disturbing the molten metal. Sampling would introduce undesirable oxides into the PoDFA crucible, resulting in an artificial increase in the filtration time. Increasing the holding periods of the molten metal increases the quantity of dross. In all cases, the skimmed dross is wet, i.e., it contains an appreciable amount of molten metal. The main types of oxides in the dross are MgO, $MgAl_2O_4$, Al_4C_3 and Al_2O_3.

1. Introduction

It is well established that a large variety of inclusions are present in small quantities in commercial aluminium and in aluminium alloys [1–5]. The results of Simensen and Berg [1] show that commercial aluminium contains mainly the following types of inclusions: 6–16 ppm oxides, 3–12 ppm nitrides (AlN), 2–12 ppm carbides (Al_4C_3) and less than 1 ppm of cryolites and borides. Grain-refined material contains normally 10–100 ppm TiB_2 and VB_2. Intermetallic phases such as Al_3Zr, AlB_2 and Al_3Ti are formed in highly alloyed melts. Using 50 μm pore size filters, Simensen and Hartvedt [6] could analyse the inclusions in Al–Fe–Si and Al–Mg commercial ingots. These ingots contained 0.1–2.2 ppm oxides (thin films and clusters of oxide particles of Al_2O_3, Al_2MgO_4 and MgO).

The work of Apelian and Mutharasan [7] shows that the production of quality castings necessitates that inclusion contents are of the order of *several volume parts per billion* and that the particle size of the population is less than 50 μm. Techniques such as sedimentation, flotation and filtration may be used to minimize the incidence of inclusions in the casting. Gravity sedimentation may be effective for inclusions larger than 90 μm. The flotation technique, i.e., degassing with inert or active gas using rotating impellers, may be effective up to about 30–40 μm, whereas filtration using ceramic foam filters is generally used to remove inclusions less than 30 μm. Applying open-pore ceramic foam filters would result in improved cleanliness and scrap reduction, increased yield and energy savings, greater productivity from the mould area, reduced machining scrap, increased tool life and reduced machining allowances, improved properties and greater assurance of quality [8–10].

The process dynamics of liquid metal filtration using reticulate ceramic filters has been analysed by Tian [11] and Tian and Guthrie [12, 13] through solving numerically the macroscopic balance equation, in conjunction with proposed correlation relating filter coefficients to the amounts of non-neutrally buoyant particles captured. The distribution of particles captured within a filter, its evolution both as a function of filtration time and melt cleanliness, together with its consequent effects on filtration efficiency and pressure drop has been simulated.

Higher aluminium quality can be expected if the furnace treatment is optimized since in-line treatment units essentially remove impurities in a proportional manner. The most widely accepted method used for furnace fluxing consists of injecting a gaseous mixture of nitrogen and chlorine (N_2–Cl_2) through stationary lances [14]. Celik and Doutre [15] showed that the volume of chlorine gas in excess of stoichiometric requirements is responsible for acid gas emissions

0022–2461

(HCl and Cl_2). Total gas flow during fluxing controls particle and inclusion emissions. Two approaches can be selected to reduce emissions associated with fluxing: abatement of emissions after they have been generated or reduction at the process source. The use of a chlorine gas furnace is already banned in a number of states and countries owing to environmental problems. The replacement of chlorine gas by more environmental-friendly fluxes is thus foreseeable in the near future [16].

Recently, it has been suggested that chlorine-free gas mixtures composed of sulphur hexafluoride (SF_6) and an inert carrier gas can be employed for both in–line and furnace fluxing [17, 18]. Emission levels measured during furnace fluxing with SF_6–N_2 mixtures were very low compared with those measured during furnace fluxing using Cl_2–N_2 mixtures. Severe oxidation which commonly occurs at the liquid metal surface of high-magnesium alloys can be effectively inhibited by use of a cover gas composed of SF_6 and N_2.

Martin and Painchaud [19] reported on the techniques required for monitoring and minimizing the presence of non-metallic inclusions of the order of parts per billion. Such low concentrations are not accessible by direct chemical analysis methods. These techniques, based on a pre-concentration–filtration step, followed by metallographic analysis, have been variously developed as Alcan's porous disc filtration apparatus (PoDFA) [20] and the Union Carbide's LAIS [21] methods. Obtaining results of inclusion testing by these methods, however, is time consuming and by the time that the results are received, the metal produced may have already left the cast house.

In Part I of the present study, we reported the effect of foundry parameters and minor alloying element additions on inclusion formation in A356.2 and C357 alloys, measured by the PoDFA technique. The obtained data has been analysed in the present part, which represents the second phase of an ongoing research program covering the study of inclusions in aluminium alloys.

2. Results and discussion

2.1. Dross formation

Dross, the oxide layer that covers the surface of molten metal, was carefully skimmed without folding, and the mass determined, as listed in Table I. As can be seen, the mass of dross varies from about 60–75 g (after melting either a fresh or scrap charge of A356.2 alloy) to about 500 g (after degassing for a short period of time (45 min)). Prolonged holding times of liquid metal at temperatures of the order of 730–740 °C also have a very significant effect on increasing the mass of the dross from about 80 g to about 525 g. This observation is independent of alloy type, i.e., A356.2 or C357.

Surfaces of dross fragments were examined macroscopically. Fig. 1(a) shows the air-exposed surface of dross taken from an A356.2 alloy melt (experiment 20A) that was held for 72 h at 735 °C. It is seen that the surface is noticeably rough, compared with the freshly formed dross (experiment 18A) taken immediately after melting. Examining the opposite surface of sample 20A (Fig. 1b) reveals a thick layer of aluminium that was removed with the dross, i.e., wet dross. Increasing the Mg content (i.e., C357 alloy) does not change the melting behaviour of Al–Si–Mg alloys, as exhibited in Fig. 2a. Some black spots are, however,

TABLE I Masses of the dross

Experiment number	Alloy	Mass of dross (g)
12	A356.2, scrap	242
13	A356.2, scrap	322
14	A356.2, fresh	480
15	A356.2, fresh	522
16	A356.2, scrap	59
17	A356.2, scrap	288
18	A356.2, fresh	74
19	A356.2, fresh	466
20 A	A356.2, fresh	187
20 B	A356.2, fresh	177
21 A	A356.2, fresh	299
21 B	A356.2, fresh	143
22 A	A356.2, fresh	221
22 B	A356.2, fresh	116
24	C357, fresh	84
25 A	C357, fresh	522
25 B	C357, fresh	73
25 C	C357, fresh	65
26 A	C357, fresh	428

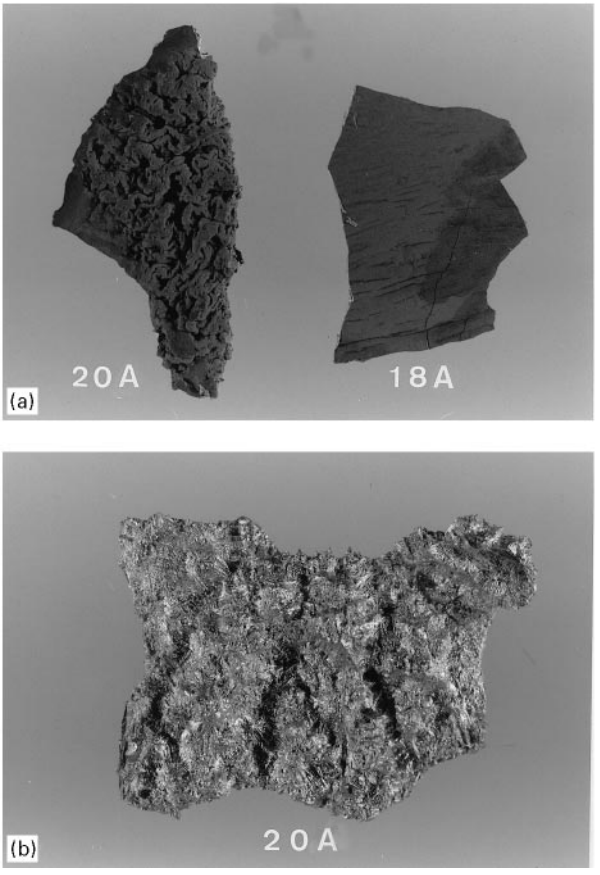

Figure 1 Morphology of the dross collected from A356.2 alloy: (a) air-exposed surface; (b) melt-exposed surface. Note the roughness of the surface when the holding time increased to 72 h.

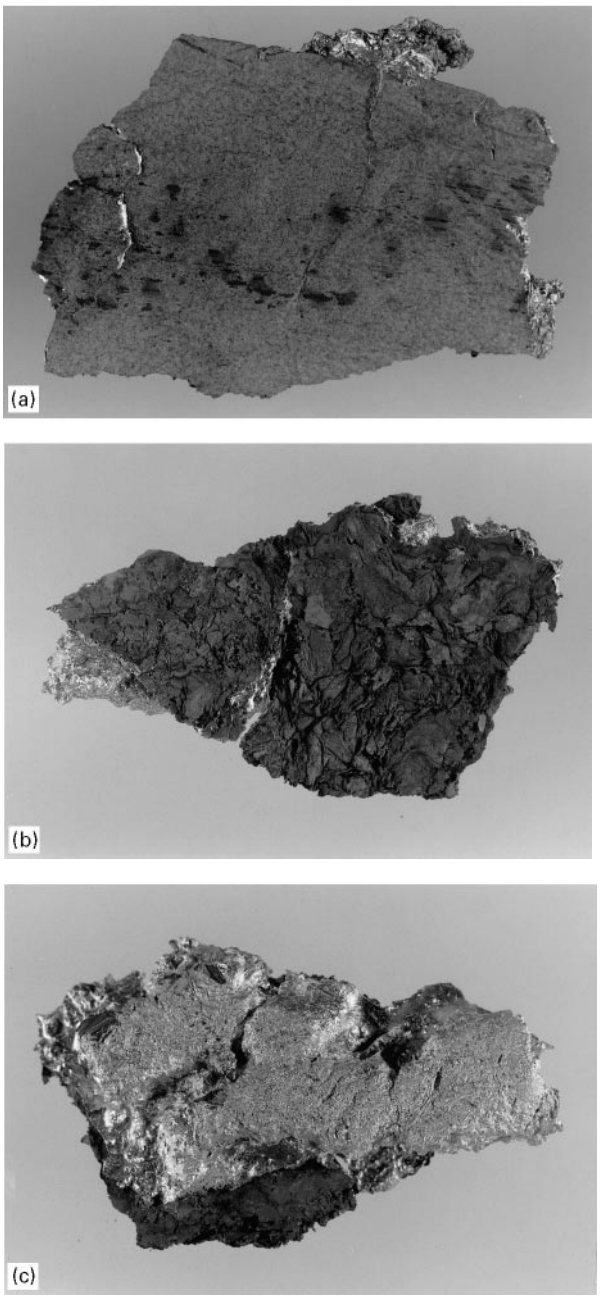

Figure 2 Morphology of the dross collected from C357 alloy: (a) experiment 24A, air-exposed surface; (b) experiment 25A, air-exposed surface; (c) experiment 25A, melt-exposed surface.

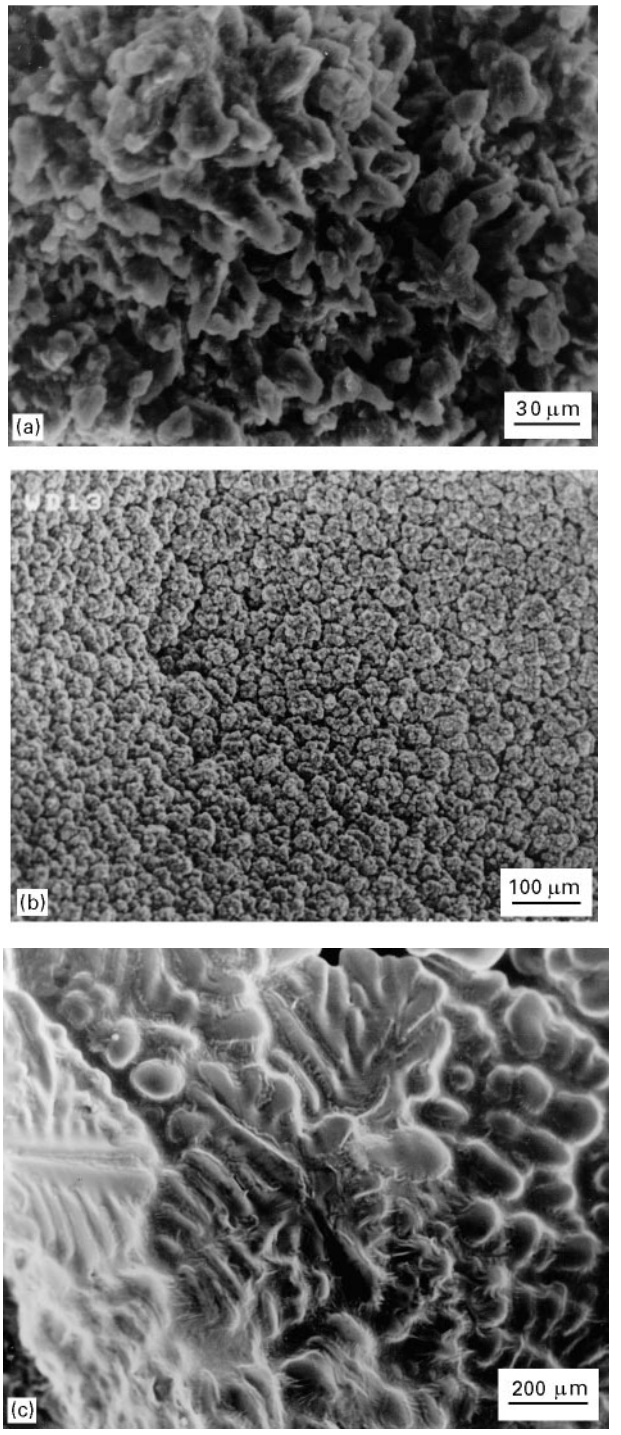

Figure 3 Scanning electron micrographs of dross collected from A356.2 alloy: (a) experiment 18A air-exposed surface; (b) experiment 20A, air-exposed surface; (c) experiment 20A, melt-exposed surface.

seen on the air-exposed surface of the dross. These spots are believed to be spinel Al_2MgO_4. Holding the liquid metal for periods as long as 72 h resulted in the formation of "ashy layers" of what looked like burnt metal. These layers were very fragile and easy to break (Fig. 2b corresponding to experiment 25A). As in the case of A356.2 alloy, a fairly thick layer of molten alloy adhered to the dross (Fig. 2c).

The same pieces of dross were examined by scanning electron microscopy (SEM) equipped with an energy-dispersive X-ray system (EDXS). In each case, about six areas (each 400×600 μm) were analysed. Fig. 3a is a scanning electron micrograph obtained from dross taken from the air-exposed surface of the melt from experiment 18 (A356.2 alloy). It is observed that the surface is not truly smooth as appears in Fig. 1a. In fact, a large number of oxide and inclusion particles appearing to grow in a columnar fashion can be seen. The corresponding energy-dispersive X-ray spectrum is given in Fig. 4a and comprises strong reflections of Al, Si, Mg and O_2 elements. It is interesting to note the presence of a carbon reflection also. The average elemental analysis of the six areas is reported in Table II. Increasing the holding time of the molten metal to 72 h (experiment 20, air-exposed surface) resulted in a granular surface (Fig. 3b), similar in nature to that presented in Fig. 1a. The

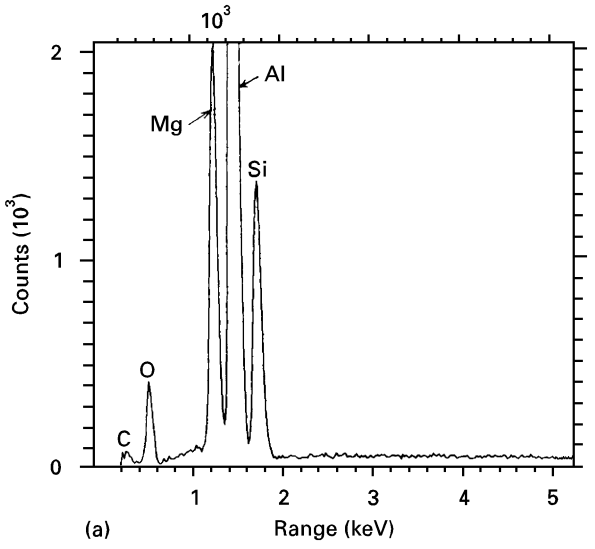

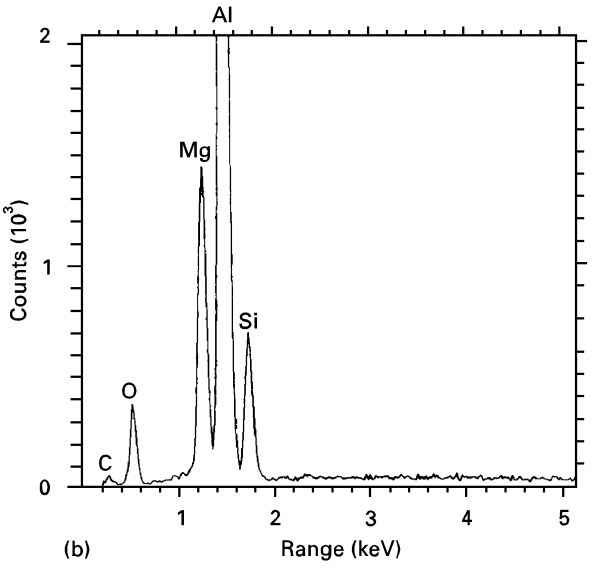

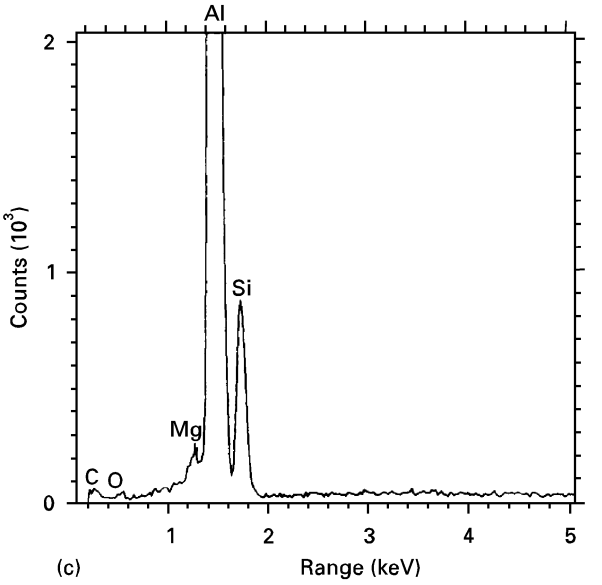

Figure 4 Energy-dispersive X-ray spectra corresponding to dross specimens of A356.2 alloy: (a) experiment 18A, air-exposed surface; (b) experiment 20A, air-exposed surface; (c) experiment 20A, melt-exposed surface.

energy-dispersive X-ray spectrum obtained from this sample is displayed in Fig. 4b and reveals lines similar to those obtained in Fig. 4a from experiment 18. The difference between the two experiments lies in the amount of collected dross (Table I). Fig. 3c exhibits the microstructure of the other side of the dross, i.e., the surface that was in contact with the molten metal, showing several dendrites. The obtained energy-dispersive X-ray spectrum (Fig. 4c), shows very low concentrations of Mg and O_2 (0.46 wt% and 0.23 wt%, respectively (Table II)) compared with those produced from the air exposed surface (20.25% and 4.48%, respectively). It is thus concluded that the air-exposed surface contains a large proportion of Al_2O_3, MgO, $MgAl_2O_4$ and Al_4C_3, whereas the melt-exposed surface is made up of mainly Al–7 wt% Si–0.35 wt% Mg base alloy.

Fig. 5a shows the roughness of the air-exposed surface of dross collected from experiment 24A (C357 alloy). It is evident from the corresponding energy-dispersive spectrum (Fig. 6a), that the concentration of oxygen in this sample is somewhat higher than the magnesium concentration (see Table II for comparison). This observation may indicate the progress of spinel formation. Prolonged holding periods of the molten metal, i.e., 72 h (experiment 25A) resulted in vigorous reactions that appeared in the form of large foam bubbles (Fig. 5b). The corresponding energy-dispersive X-ray spectrum is shown in Fig. 6b, where strong oxygen, magnesium and aluminium reflections can be seen. The reflection from

TABLE II Elemental analysis of the dross using EDXS (window size, 400 μm × 600 μm)

Alloy	Experiment number	Surface	Settling time (h)	Amount (at%) of the following elements				
				C	O	Mg	Al	Si
A356.2	18	Air	0	0.64	3.87	22.17	64.3	9.03
A356.2	18	Melt	0	0.11	4.89	1.5	73.01	20.49
A356.2	20	Air	72	0.75	4.48	20.25	68.39	6.13
A356.2	20	Melt	72	0.15	0.23	0.46	92.77	6.4
C357	24	Air	0	0.62	36.56	8.06	51.22	3.54
C357	24	Melt	0	0.08	0.22	0.61	91.56	7.58
C357	25 A	Air	72	0.2	15.98	35.07	47.46	1.29
C357	25 B	Air	—	0.15	7.16	24.25	64.11	4.34
C357	25 C	Air	—	0.14	5.2	12.03	76.35	6.53

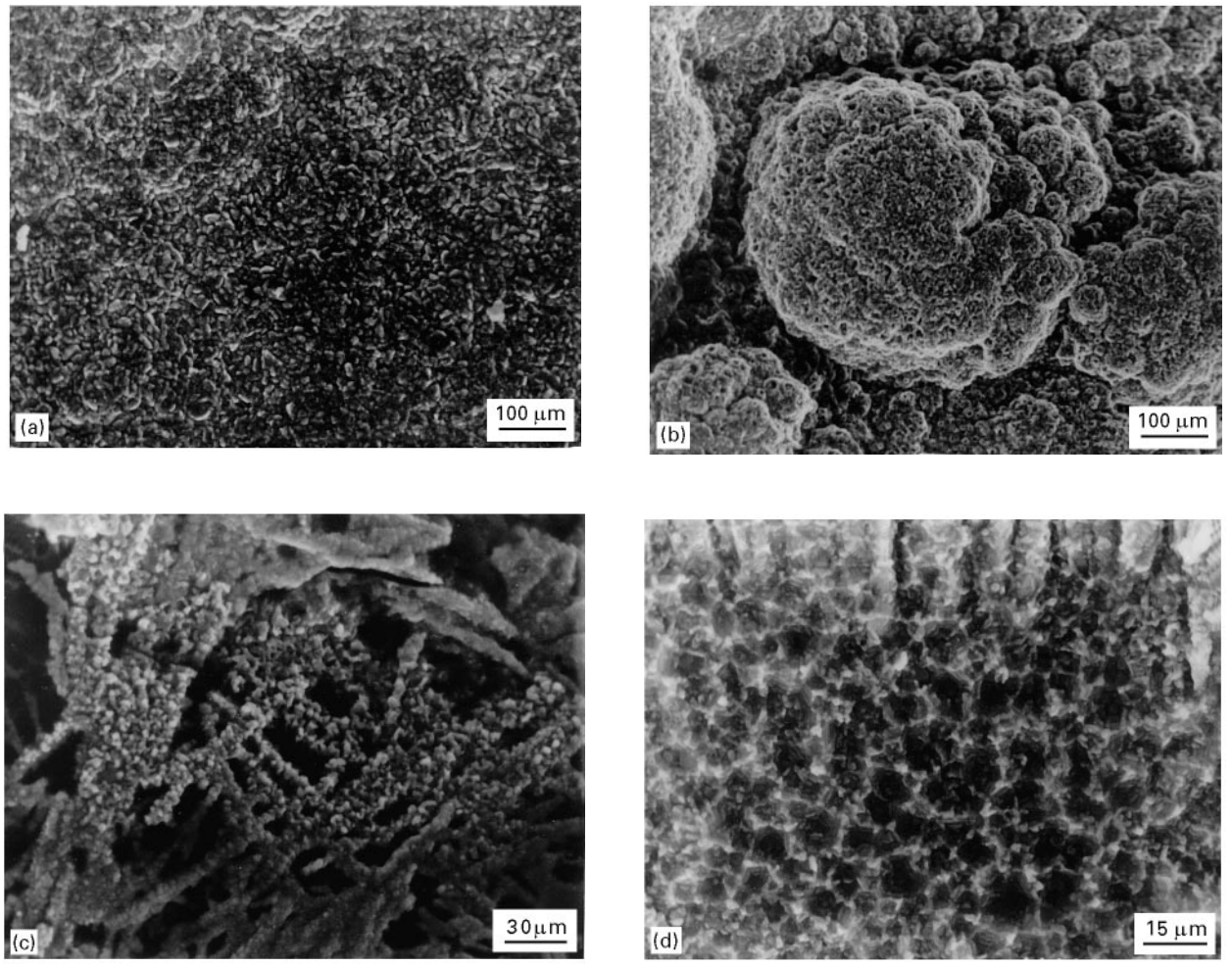

Figure 5 Scanning electron micrographs of dross collected from C357 alloy: (a) experiment 24A, air-exposed surface; (b) experiment 25A, air-exposed surface; (c) experiment 25A, air-exposed surface; (d) experiment 25C, air-exposed surface.

silicon is relatively negligible. Another morphology of spinel phase particles is displayed in Fig. 5c. In this case the spinel occurred in the form of a bundle of sticks covered with fine particles. The associated energy-dispersive X-ray spectrum (Fig. 6c) did not reveal any special features apart from those reported earlier, and the energy-dispersive X-ray spectrum produced from the molten-metal-exposed surface displayed reflections corresponding to the base alloy (Fig. 6d).

The morphology of freshly formed spinel (i.e., immediately after skimming) is shown in Fig. 5d, when the remaining melt was degassed with inert gas for about 45 min. The spinel seems to form some sort of a cellular structure in this case, with fine particles decorating the cell boundaries. It is of interest to observe from the associated energy-dispersive X-ray spectrum (Fig. 6e) the noticeable increase in the intensity of the silicon reflection, indicating the ability of the X-ray beams to penetrate the entire oxide layer and to reach the molten metal layer underneath. In other words, the oxide layer is relatively thin compared with that obtained from experiment 25A (see Table I). The concentration of silicon is seen to increase progressively as listed in Table II, resulting from the continuous decrease in the thickness of the oxide layer.

2.2. Inclusion–filtration time relationships

2.2.1. Cold chamber

Inclusion concentrations have been classified arbitrarily into five categories as listed in Table III, whereas oxide films have been divided into seven classes following Alcan's procedure.

As expected, when the pressure chamber [22] is not pre-heated prior to executing the PoDFA trial, the minimum time required to filter about 1.5 kg of molten metal is about 5 min. The maximum inclusion concentration was of the order of 0.06 $mm^2\ kg^{-1}$, an amount considered to be very low to cause such an extended filtration time. It was evident that a cold chamber would result in shorter solidification times and lower fluidities, parameters accounting for lengthy filtration periods.

From the total harmful inclusions (i.e., after subtracting fine (3 μm or less) Al_4C_3 TiB_2 and potential chloride particles) a very low concentration of the order of 0.01 $mm^2\ kg^{-1}$ could increase the filtration time to approximately 10 min. As could be seen from Tables IX-XI in Part I, under these filtration conditions, oxide films of class (2), i.e., thin/moderate could cause considerable filtration delay.

According to the classification shown in Table III all inclusions fall into the category 'very light'. Thus the

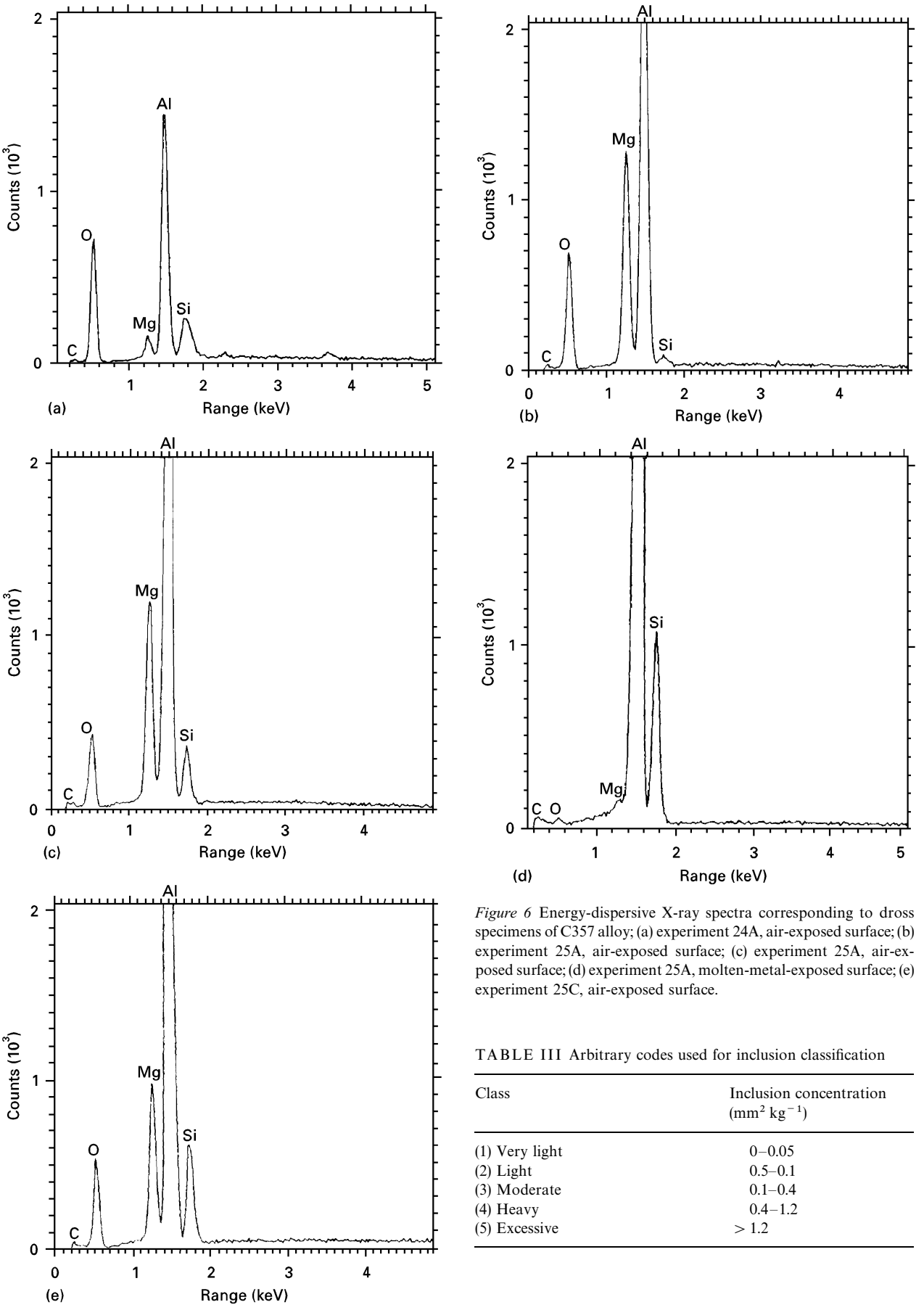

Figure 6 Energy-dispersive X-ray spectra corresponding to dross specimens of C357 alloy; (a) experiment 24A, air-exposed surface; (b) experiment 25A, air-exposed surface; (c) experiment 25A, air-exposed surface; (d) experiment 25A, molten-metal-exposed surface; (e) experiment 25C, air-exposed surface.

TABLE III Arbitrary codes used for inclusion classification

Class	Inclusion concentration ($mm^2\ kg^{-1}$)
(1) Very light	0–0.05
(2) Light	0.5–0.1
(3) Moderate	0.1–0.4
(4) Heavy	0.4–1.2
(5) Excessive	> 1.2

solidification time plays a more influential role than inclusions in determining the filtration time. It should be noted, however, that the presence of very small quantities of TiB_2 (about 0.007–0.01 $mm^2\ kg^{-1}$) could also contribute to the observed long filtrations times.

2.2.2. Hot chamber

2.2.2.1. Effect of foundry parameters. The variation in filtration time as a function of total inclusion content, when the pressure chamber was pre-heated using two empty PoDFA crucibles heated at 850 °C is displayed in Fig. 7a. When the inclusion concentration falls

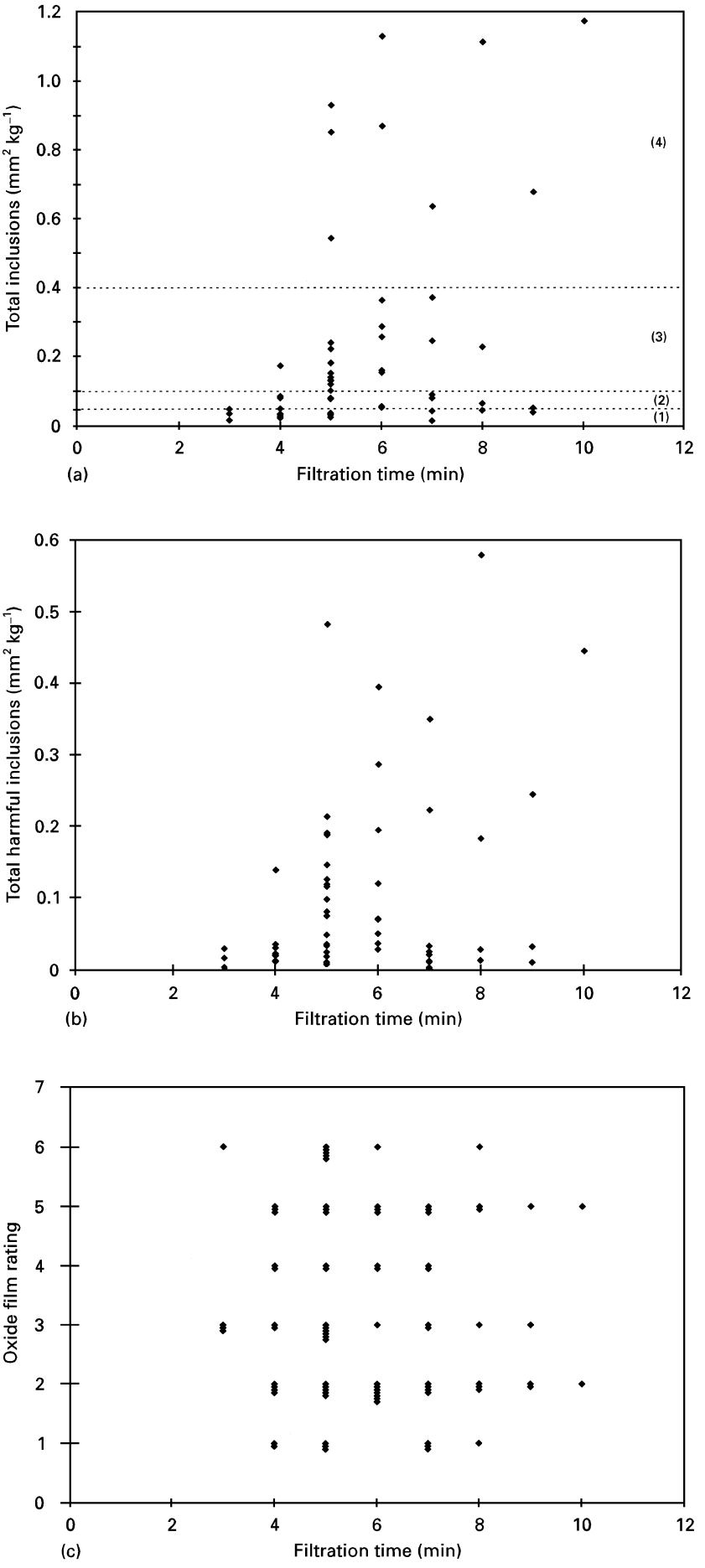

Figure 7 Dependence of filtration time on inclusion concentrations and oxide films (hot chamber): (a) total inclusions; (b) total harmful inclusions; (c) oxide film rating.

within the range classified as very light (Table III), the filtration time is about 3 min. Increasing the total inclusion concentrations to 0.1 $mm^2\ kg^{-1}$ or more would obviously lead to filtration times varying between 5 and 10 min, depending on the concentration of harmful inclusions (Fig. 7b), and, more importantly, on the type of oxide film (Fig. 7c). Based on the data presented later in Fig. 9c, it may be concluded that, under appropriate filtration conditions, and for low concentrations of inclusions (around 0.1 $mm^2\ kg^{-1}$ or less), larger amounts of oxides (Alcan classification: level 6 (see Table IV)) could be tolerated to obtain a certain filtration time (e.g., 5 min).

It should be borne in mind that oxide films can easily be trapped in the unfiltered metal during sampling if the necessary precautions are not strictly followed. Turbulence of the molten metal, however, cannot be totally avoided during either filling of the ladle or pouring of the liquid metal into the PoDFA crucible. Also, using red-hot (about 850 °C) PoDFA crucibles could certainly introduce, to some extent, oxide layers that may cause filtration problems in later stages. Another parameter to be considered is the distance between the melting furnace and the PoDFA apparatus. The shortest distance possible is recommended.

The dependence of filtration time on inclusion content has been divided into four major classes (according to their industrial importance) following the arbitrary classification shown in Table III. The variation in filtration time as a function of inclusion concentration in the range 0–0.05 $mm^2\ kg^{-1}$, i.e., very light, is shown later in Fig. 10. The data in Fig. 10a can be divided into two sets: 3–5 min which represents the major number of samples, and 7–9 min which includes only a few samples. This separation is mainly based on the type(s) of oxide film found in each sample. As reported earlier in Part I of this work, each sample contained certain amounts of both types of oxide film, i.e., thin and thick. Thus, on the basis of the foregoing discussion, it seems that the type of oxide film in the sample is the deciding parameter that controls the filtration time.

The effect of inclusion concentration in the range 0.05–0.1 $mm^2\ kg^{-1}$ on filtration time is shown in Tables IX–XI in Part I. Two main observations could be drawn from these tables.

(a) In the presence of thin/light or thin/moderate oxide films, inclusion contents of the order of 0.08 $mm^2\ kg^{-1}$ could lead to filtration times as high as 7 min.

(b) For a relatively low inclusion concentration of about 0.05 $mm^2\ kg^{-1}$, the presence of the thick/moderate or thick/heavy type of oxide films is detrimental.

It is evident that without metallographic examination, it is very difficult to evaluate the effect of each parameter.

The dependence of filtration time on inclusion content in the range 0.1–0.4 $mm^2\ kg^{-1}$ (termed moderate in Table IV) is displayed in Tables IX and X in Part I. Most of the experiments are clustered in the range 5–7 min. It should be noted that the total harmful inclusions (SONIM) could be as low as

TABLE IV Codes used for oxide film classification (Alcan's procedure)

Class	Oxide film type/density
0	None
1	Thin/slight
2	Thin/moderate
3	Thin/heavy
4	Thick/slight
5	Thick/moderate
6	Thick/heavy

0.02 $mm^2\ kg^{-1}$, i.e., a large proportion of inclusions is fine Al_4C_3 particles of 3 μm or less. Oxide films, on the other hand, are fairly thick (moderate and heavy) which results in significantly longer filtration times.

When the inclusion contents are higher than 0.4 $mm^2\ kg^{-1}$, filtration times can easily be as long as 10 min, although only about half of this concentration is considered harmful to the mechanical properties. This series of samples was characterized by a higher volume fraction of oxide films which result from the mechanical stirring of the molten metal prior to executing the PoDFA trials.

2.2.2.2. Effect of minor additions. Because mechanical stirring is used to ensure complete dissolution of the alloying elements added, the inclusions and oxides that settle at the bottom of the melting crucible are disturbed. Thus, it is expected that the concentration of inclusions should be relatively higher in this case than that reported earlier, for similar experimental conditions. Fig. 8a indicates that the inclusions possibly have concentrations greater than 0.4 $mm^2\ kg^{-1}$. Most of these inclusions are considered harmful from the mechanical properties standpoint (Fig. 8b). Another important point to note is that the oxide films are mainly thick/heavy as shown in Fig. 8c.

2.3. Inclusion–fluidity relationships

Various types of test devices have been used by several investigators to study the variables affecting fluidity of metals and alloys. Among these is the vacuum fluidity test developed by Ragone *et al.* [23] to study the variables affecting fluidity. It has been reported [24, 25] that this technique is considered to be a very reliable and sensitive method for studying the effect of melt composition, metal temperature and trace elements. The work of Venkateswaran *et al.* [26] shows that the fluidity of eutectic Al–Si alloys decreases with the addition of Na, Na + Sr, Ti, Na + Ti or Na + Sr + Ti, whereas the addition of Sb, S, Sb + Ti or P + Ti increases the fluidity of the eutectic aluminium–silicon alloys.

The dependence of fluidity (measured by the length of solidified metal in the quartz tube of the Ragone fluidity tester) on the inclusions content is explained in Fig. 9a. The average length of solidified metal is about 36 ± 2 cm, regardless of the concentration of total

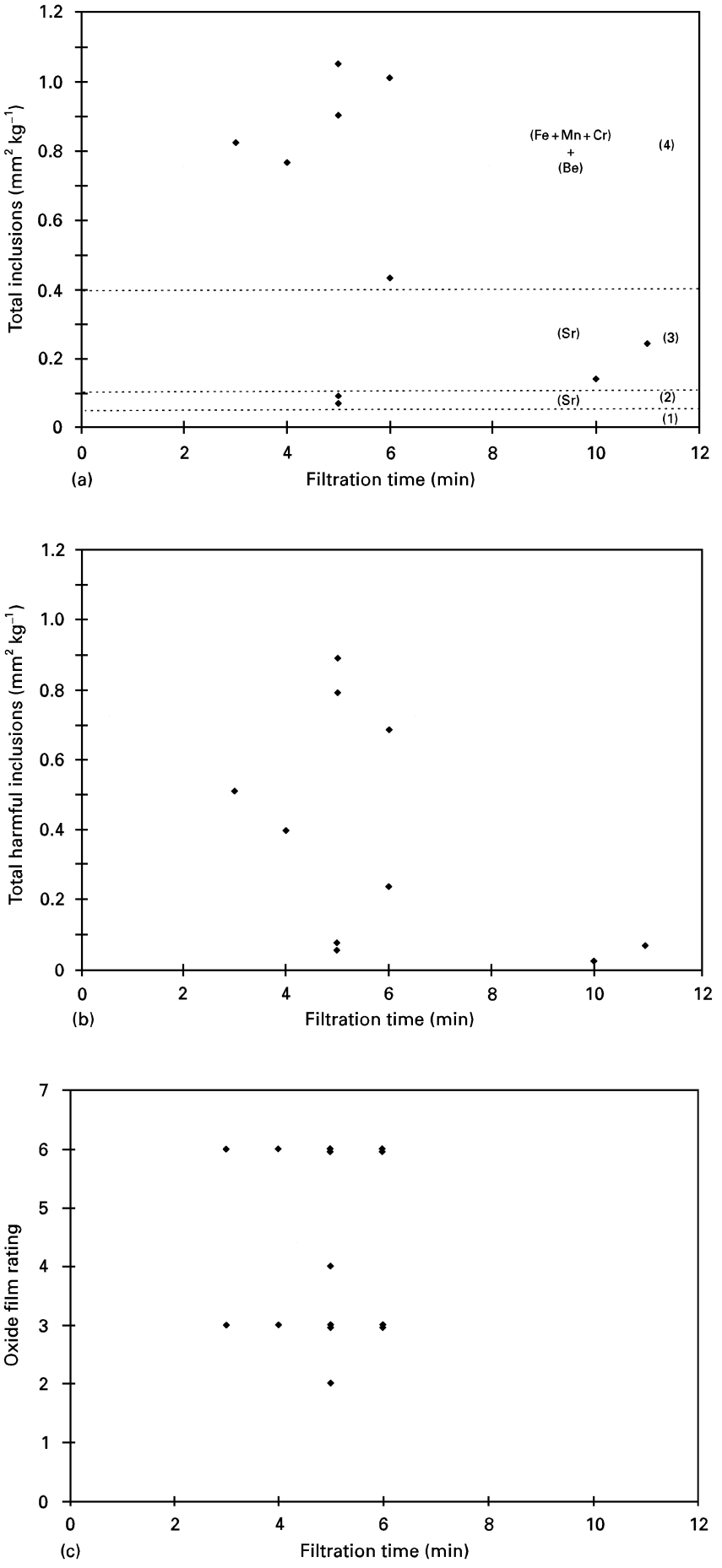

Figure 8 Dependence of filtration time on inclusions caused by minor element additions (hot chamber): (a) total inclusions; (b) total harmful inclusions; (c) oxide film rating.

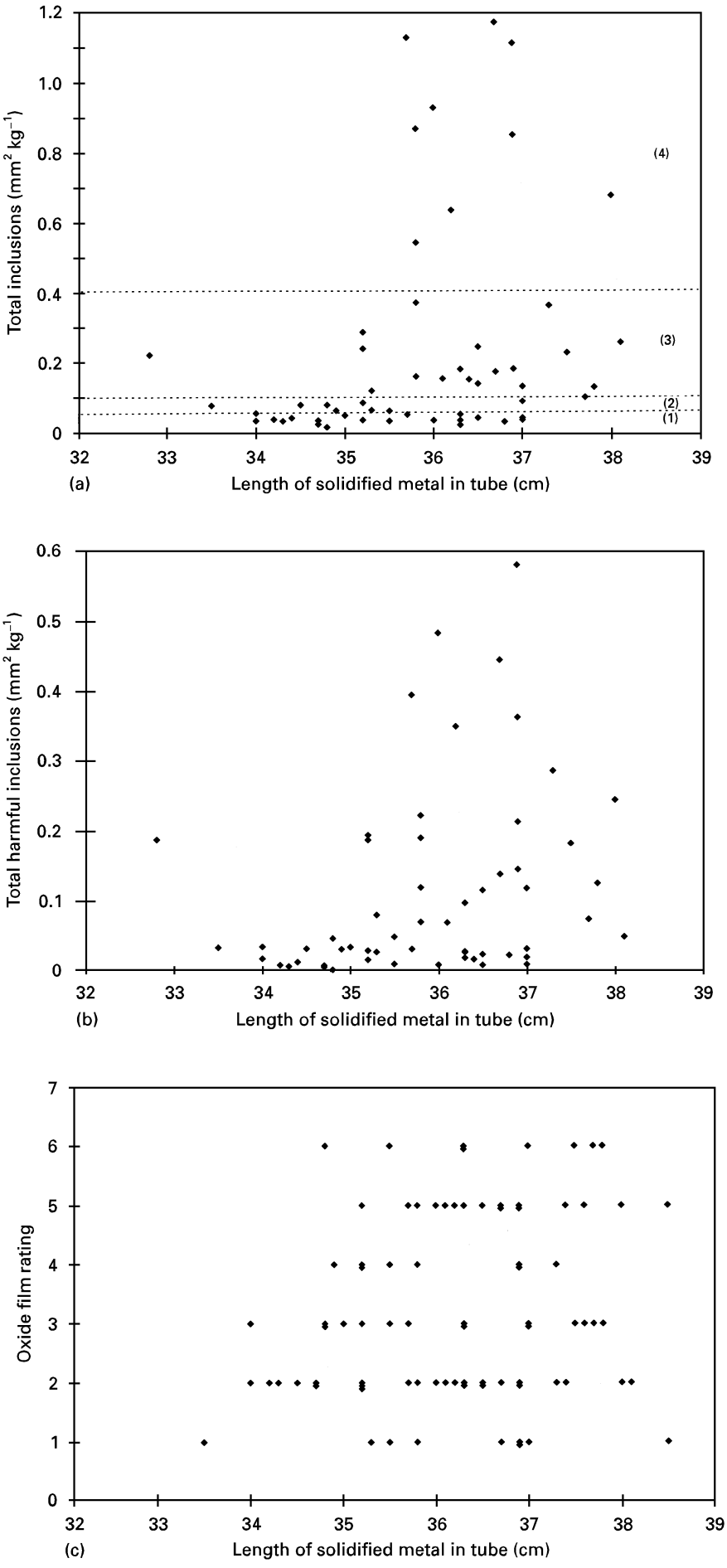

Figure 9 Dependence of the length of solidified metal obtained in the Ragone fluidity test tube on inclusions caused by variations in the foundry parameters: (a) total inclusions; (b) total harmful inclusions; (c) oxide film rating.

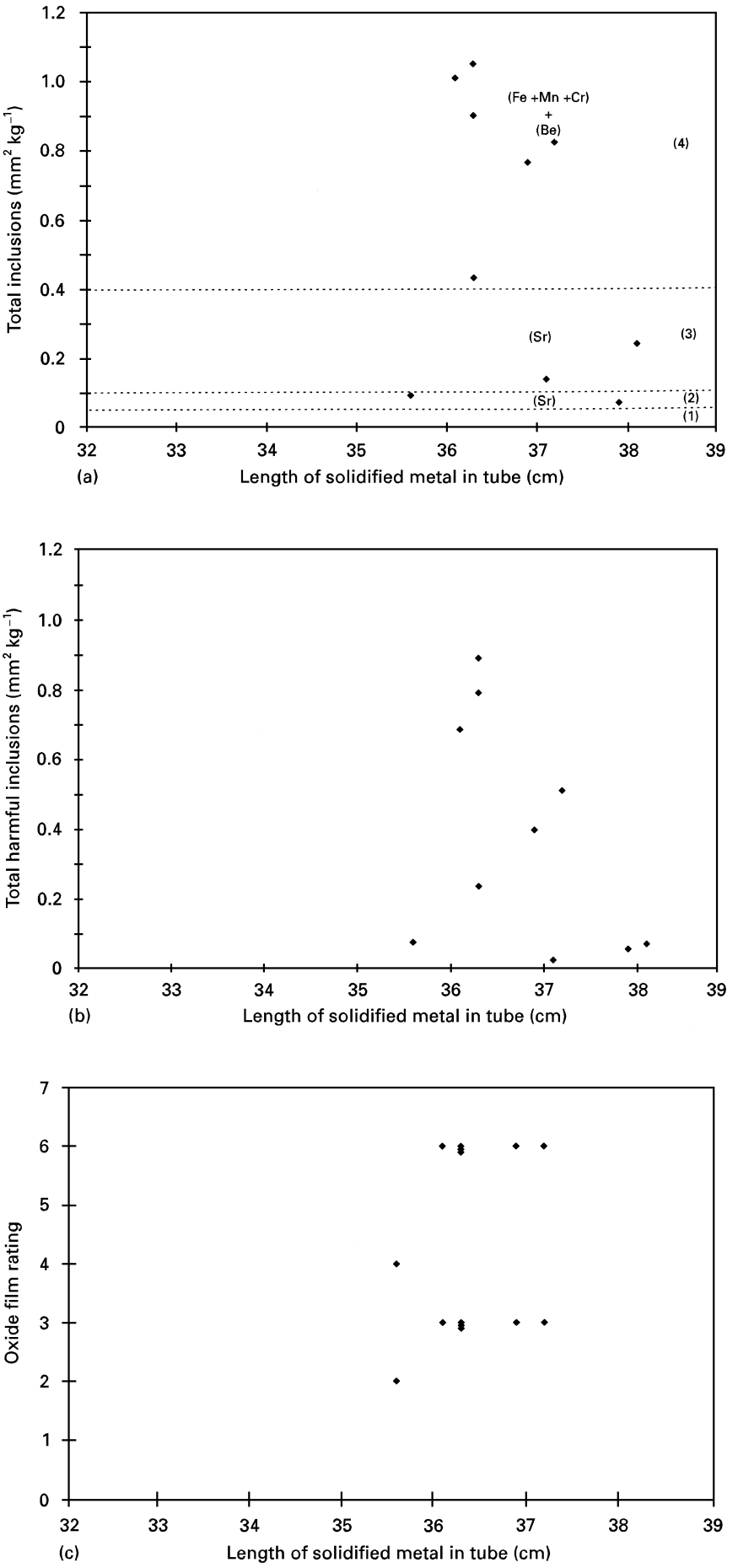

Figure 10 Dependence of the length of solidified metal obtained in the Ragone fluidity test tube on minor element additions (hot chamber): (a) total inclusions; (b) total harmful inclusions; (c) oxide film rating.

inclusions in the range 0–1.2 $mm^2\ kg^{-1}$. Considering the total harmful inclusions (Fig. 9b), they do not result in a noticeable change in the general distribution. It should be noted, however, that the inclusions for the majority of the measured samples fall in the range 0–0.2 $mm^2\ kg^{-1}$. The observed discrepancy in Figs 9a and b may be explicable in terms of the distribution of oxide films shown in Fig. 9c. It is rather difficult to separate the individual effect of each of the two main parameters, i.e., inclusion concentrations and oxide films on the alloy fluidity.

The data on the role of minor additions is relatively limited (Fig. 10a). Modification with Sr appears to improve the alloy fluidity noticeably (Fig. 10b), whereas oxide films associated with the addition of Fe + Mn + Cr decrease the length of solidified metal obtained. The three elements were added in the form of Al–25 wt% (Fe, Mn, Cr) master alloys. Therefore, the actual quantity of added material is almost four times that needed to achieve the required element composition. This operation would certainly create more oxide films than would be expected if pure elements were used. However, since the dissolution of pure elements is relatively very sluggish at 735 °C, the technique of using master alloys is preferred instead.

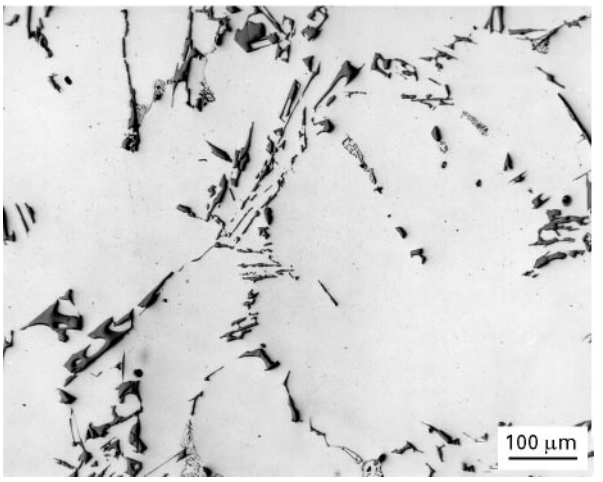

Figure 11 Microstructure of base alloy away from the inclusion cake.

2.4. Examples of inclusion concentrations

Figure 11 shows the microstructure of the base alloy away from the inclusion cake (i.e., taken from an area above the PoDFA sample). No traces of inclusions or oxides can be seen. A typical example of what is termed as a very light inclusion level (i.e., 0–0.05 $mm^2\ kg^{-1}$) is displayed in Fig. 12a, consisting

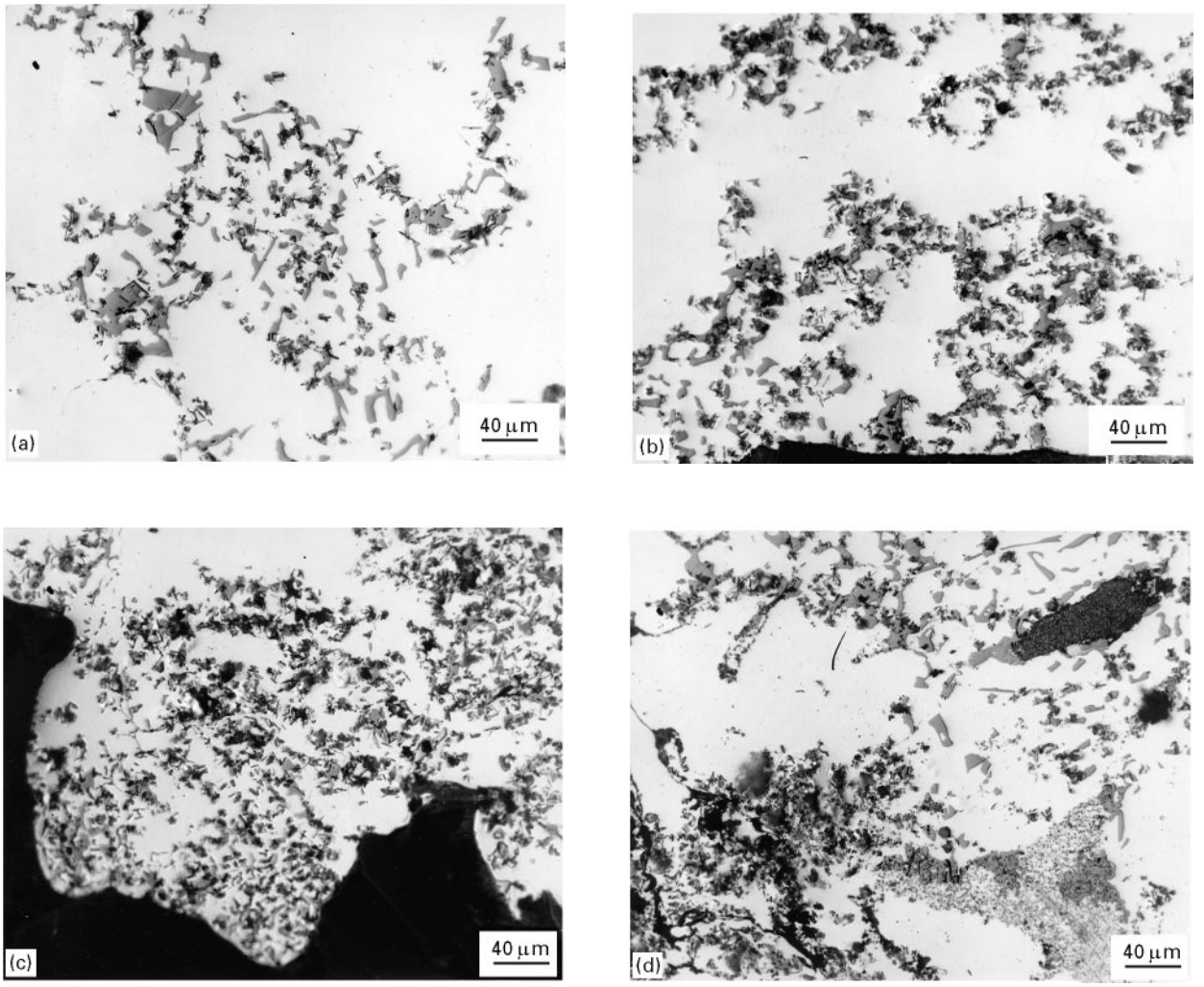

Figure 12 Examples of inclusion concentrations: (a) very light, experiment 4A; (b) light, experiment 1D, (c) moderate, experiment 15E; (d) heavy, experiment 12C; (e) excessive, experiment 29H; (f) excessive, experiment 29I.

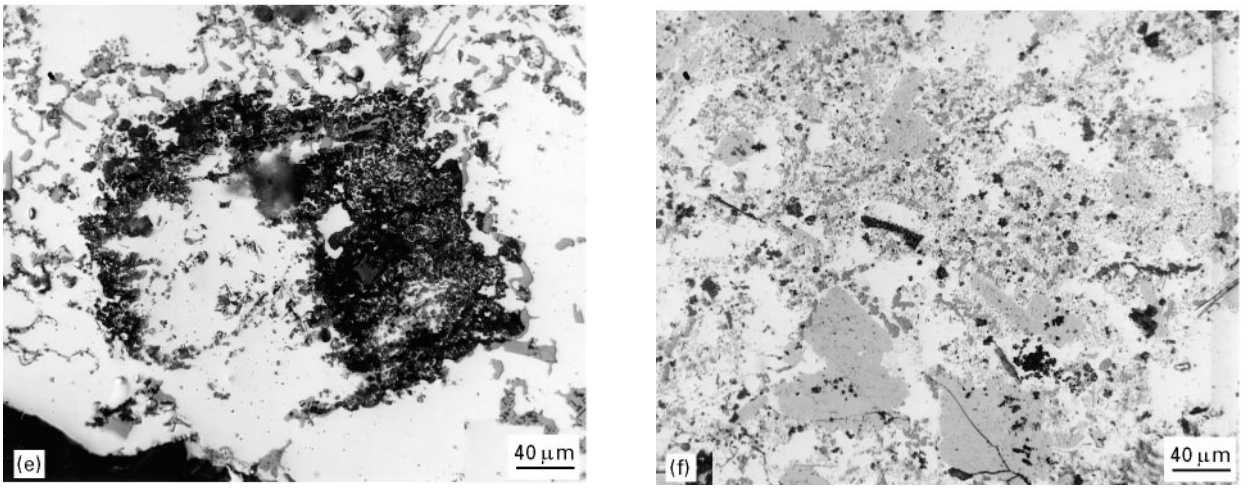

Figure 12 (Continued)

mainly of fine (≤ 3 μm) Al_4C_3. Inclusion contents in the range 0.05–0.1 $mm^2\,kg^{-1}$ (termed 'light') are presented in Fig. 12b. Although the inclusions are mainly fine Al_4C_3, some long needles of Al_4C_3 (3 μm or greater) can be observed. Inclusions classified as moderate are exemplified in Fig. 12c. They are a mixture of fine Al_4C_3 (3 μm or less), Al_4C_3 (3 μm or greater) and MgO. Note how the inclusions clog the filter pores (leading to a lengthy time of filtration). An example of heavy inclusion concentration is shown in Fig. 12d. In this case, almost all types of inclusions are present (Al_4C_3

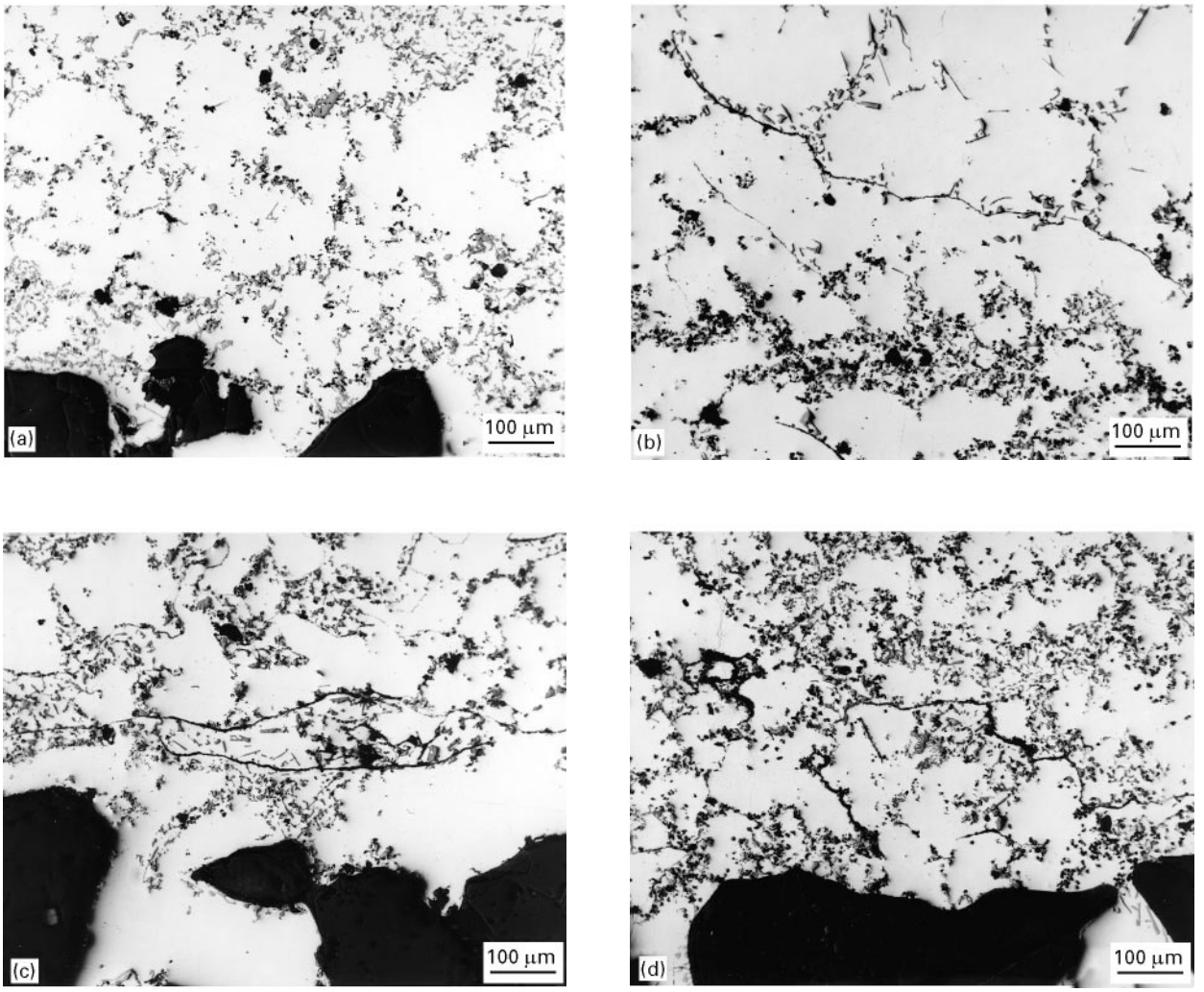

Figure 13 Examples of Al_2O_3 films and particles: (a) none, experiment 3E; (b) Thin/light, experiment 1D; (c) thin/moderate, experiment 1A; (d) thin/heavy, experiment 1B; (e) thick/light, experiment 15E; (f) thick/moderate, experiment 14E; (g) thick/heavy, experiment 7E.

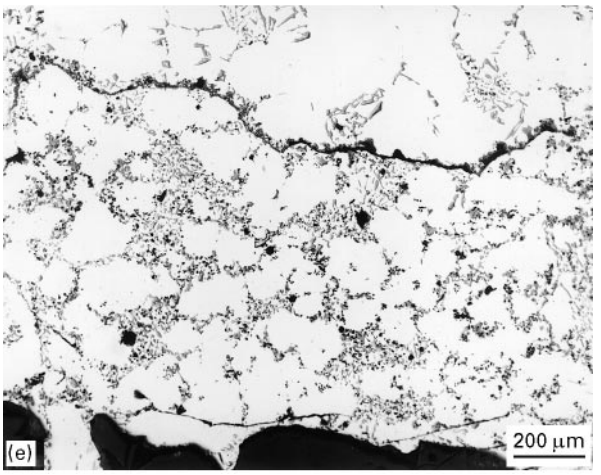

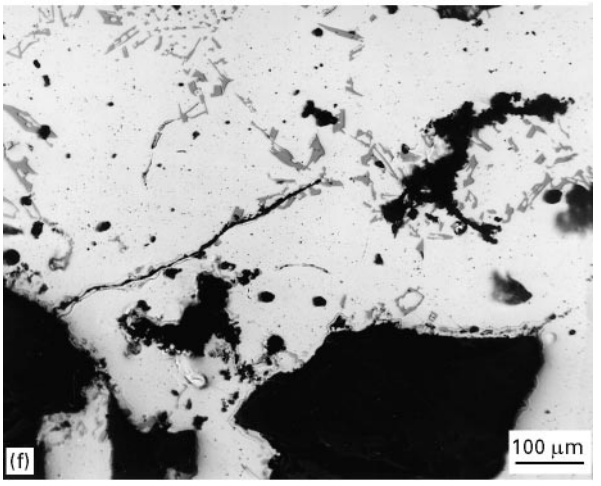

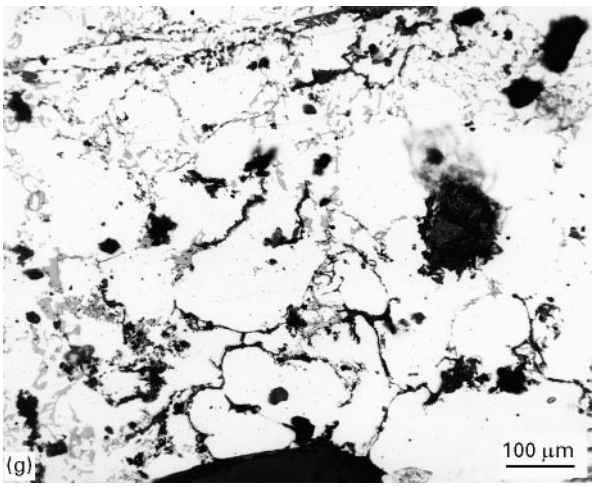

Figure 13 (Continued)

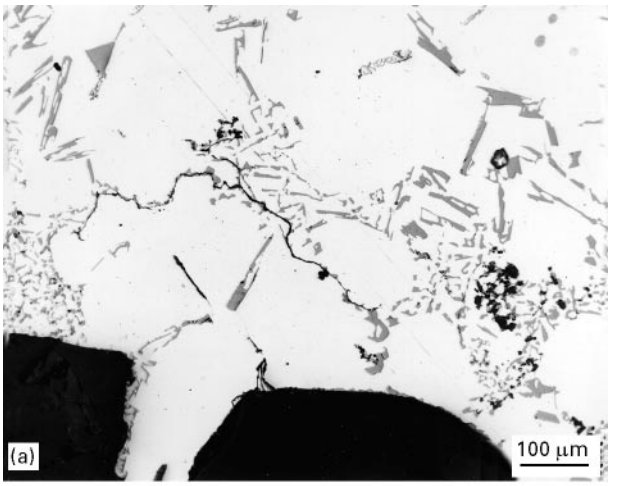

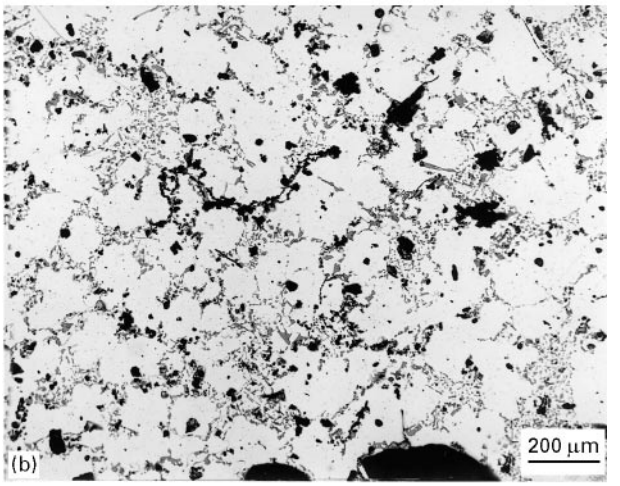

Figure 14 Effect of Al_2O_3 density on filtration time: (a) experiment 2E, 3 min; (b) experiment 7A, 5 min.

(3 μm or less), Al_4C_3 (greater than 3 μm), MgO and $MgAl_2O_4$).

When the inclusion concentration exceeds 1.2 $mm^2\ kg^{-1}$, i.e., excessive, it is rather difficult to count their concentrations accurately. It should be borne in mind that the accuracy of measurements using the grid method ranges from $\pm 15\%$ (for light to moderate) to $\pm 25\%$ (for heavy to excessive). Figures 12e and 12f are two examples of such high inclusion densities. The sedimentation of the sludge crystals (grey colour) contributes to the accumulation of TiB_2 inclusions, leading to the blocking of their passage to

TABLE AI Explanation of codes used in the present work

Code	Explanation								
C01	C: C357	0: settling time is 0 h						1: sample 1	
C41	C: C357	4: settling time is 4 h						1: sample 1	
C71	C: C357	7: settling time is 72 h						1: sample 1	
C71H	C: C357	7: settling time is 72 h	H: superheat					1: sample 1	
CS1	C: C357			S: Sr				1: sample 1	
CSTB1	C: C357			S: Sr	TB: TiB_2			1: sample	
CTB1	C: C357			TB: TiB_2				1: sample 1	
CT1	C: C357			T: Ti				1: sample 1	
CF1	C: C357			F: Fe, Mn, Cr				1: sample 1	
CFB1	C: C357			F: Fe, Mn, Cr	B: Be			1: sample 1	
CFBS1	C: C357			F: Fe, Mn, Cr	B: Be	S: Sr		1: sample 1	
CFBST1	C: C357			F: Fe, Mn, Cr	B: Be	S: Sr	T:Ti	1: sample 1	
FBST1B				F: Fe, Mn, Cr	B: Be	S: Sr	T:Ti	1: sample	B: TiB_2

TABLE AII Chemical compositions of C357 under different melt treatment conditions

Alloy code	Amount (wt%) of the following elements Si	Fe	Cu	Mn	Mg	Cr	Ni	Zn	Ti	Sn	Be	Sr	V
C01	7.06	0.0485	0.012	0.007	0.556	< 0.000	0.006	0.001	0.143	< 0.0000	0.0171	0.0015	0.00615
C41	7.06	0.049	0.012	0.008	0.576	< 0.000	0.007	0.002	0.138	< 0.0000	0.0157	0.0013	0.0062
C71	7.16	0.047	0.032	0.005	0.524	< 0.000	0.006	< 0.000	0.138	< 0.0000	0.0035	0.0011	0.006
C71H	7.19	0.048	0.032	0.005	0.516	< 0.000	0.007	< 0.000	0.139	< 0.0000	0.005	0.0012	0.0064
CS1	7.17	0.043	0.013	0.005	0.556	< 0.000	0.007	0.001	0.135	< 0.0000	0.0276	0.0238	0.0057
CSTB1	7.2	0.047	0.013	0.005	0.568	< 0.000	0.007	0.002	0.162	< 0.0000	0.0272	0.0374	0.0061
CTB1	7.44	0.049	0.012	0.005	0.554	< 0.000	0.007	< 0.000	0.156	< 0.0000	0.0384	0.02	0.006
CT1	7.07	0.049	0.012	0.005	0.564	< 0.000	0.007	0.002	0.171	< 0.0000	0.0363	0.0011	0.0063
CF1	6.9	0.304	0.0125	0.304	0.5615	0.119	0.007	0.002	0.133	< 0.0000	0.0289	0.00105	0.00595
CFB1	6.98	0.632	0.012	0.36	0.546	0.117	0.007	0	0.131	< 0.0000	0.0561	0.0011	0.0061
CFBS1	6.83	0.623	0.013	0.358	0.547	0.114	0.007	0.001	0.13	< 0.0000	0.0574	0.0215	0.006
CFBST1	6.95	0.627	0.013	0.357	0.545	0.115	0.007	0	0.149	< 0.0000	0.0534	0.0202	0.0058
FBST1B	6.92	0.643	0.013	0.365	0.556	0.117	0.007	0.002	0.162	< 0.0000	0.055	0.022	0.006

TABLE AIII Concentrations of additives in C357 alloy

Alloy code	Amount (wt%) of the following element Si	Fe	Cu	Mn	Mg	Cr	Ni	Zn	Ti	Sn	Be	Sr	V
C41	0	0.0005	0	0.001	0.02	0	0.001	0.001	− 0.005	0	− 0.0014	− 0.0002	0.00005
C71	0.1	− 0.0015	0.02	− 0.002	− 0.032	0	0	− 0.001	− 0.005	0	− 0.0136	− 0.0004	− 0.00015
C71H	0.13	− 0.0005	0.02	− 0.002	− 0.04	0	0.001	− 0.001	− 0.004	0	− 0.0121	− 0.0003	0.00025
CS1	0.11	− 0.0055	0.001	− 0.002	0	0	0.001	0	− 0.008	0	0.0105	0.0223	− 0.00045
CSTB1	0.14	− 0.0015	0.001	− 0.002	0.012	0	0.001	0.001	0.019	0	0.0101	0.0359	− 0.00005
CTB1	0.38	0.0005	0	− 0.002	− 0.002	0	0.001	− 0.001	0.013	0	0.0213	0.0185	− 0.00015
CT1	0.01	0.0005	0	− 0.002	0.008	0	0.001	0.001	0.028	0	0.0192	− 0.0004	0.00015
CF1	− 0.16	0.2555	0.0005	0.297	0.0055	0.119	0.001	0.001	− 0.01	0	0.0118	− 0.00045	− 0.0002
CFB1	− 0.08	0.5835	0	0.353	− 0.01	0.117	0.001	− 0.001	− 0.012	0	0.039	− 0.0004	− 0.00005
CFBS1	− 0.23	0.5745	0.001	0.351	− 0.009	0.114	0.001	0	− 0.013	0	0.0403	0.02	− 0.00015
CFBST1	− 0.11	0.5785	0.001	0.35	− 0.011	0.115	0.001	− 0.001	0.006	0	0.0363	0.0187	− 0.00035
FBST1B	− 0.14	0.5945	0.001	0.358	0	0.117	0.001	0.001	0.019	0	0.0379	0.0205	− 0.00015

TABLE BI Filtering parameters and fluidity of C357 alloy

Experiment number	Mass of filtered metal (kg)	Filtration time (min)
24A	1.528	4
24B	1.531	3
24C	1.525	3
24D	1.381	3
24E	1.168	3
24F	1.509	3
24G	1.481	3
24H	1.379	4
25A	1.567	3
25B	1.473	4
25C	1.487	5
25D	1.32	5
25F	1.127	5
25G	1.412	4
25H	0.938	3
26A	1.488	3
26B	1.231	3
26C	0.842	3
26D	0.252	8
26E	0.512	5
26F	0.245	6
26G	0.263	12
26H	0.245	6
27A	0.35	7
27B	0.353	9
27C	0.452	10
27D	0.401	9
28A	1.442	4
28B	1.014	4
28C	1.514	3
28D	1.507	5
29A	1.566	3
29B	1.348	3
29C	1.374	5
29D	1.158	3
29E	1.178	5
29F	1.255	5
29G	1.169	4
29H	1.233	5
29I	0.293	6

the filter pores as seen in Fig. 12(f). Details of the inclusions are listed in Table 4 and are also given in Appendix A and Appendix B.

2.5. Examples of oxide films

Figures 13a–g show different types of aluminium oxide (Al_2O_3) either in the form of films (thin or thick) or as dark (black) patches with irregular shapes. The ratings reported in the present study are based on the classification procedure defined by the Research and Development Centers of Alcan International Limited. Note that, in most of the cases, the oxide films tend to precipitate towards the metal–filter interface as seen in Fig. 13g.

The effect of oxide density on filtration time is well demonstrated in Fig. 14. When the Al_2O_3 occurs in the form of pencil-like lines (Fig. 14a arrowed) the filtration time is about 3 min or less (total inclusions about 0.015 $mm^2\,kg^{-1}$). The presence of thick/heavy oxide films, as well as oxide particles in Fig. 14b increases the filtration time to 5 min (total inclusions, about 0.044 $mm^2\,kg^{-1}$). Such a delay was commonly observed when the molten metal was disturbed during sampling or if skimming (i.e., removal of the oxide layer prior to sampling) was not properly carried out.

TABLE BII Total and harmful inclusion concentrations in C357 alloy

Experiment number	Total inclusions ($mm^2\,kg^{-1}$)	Harmful inclusions ($mm^2\,kg^{-1}$)
24B	0.387	0.349
24D	0.452	0.416
24E	0.28	0.252
24H	0.822	0.74
25A	0.446	0.446
25D	0.493	0.395
25E	0.84	0.714
25G	1.292	0.905
26A	0.729	0.729
26C	0.77	0.462
26D	11.564	1.041
26E	4.257	0.255
26H	8.311	0.582
27B	8.618	0.862
27C	11.695	1.754
27D	12.06	1.447
28A	0.948	0.863
28D	2.271	0.954
29A	2.157	1.596
29B	2.314	1.805
29C	2.592	2.048
29D	1.104	0.773
29E	1.488	1.235
29F	1.574	1.102
29H	1.954	1.387
29I	12.766	2.809

3. Conclusions

From the analysis of the inclusions observed in A356.2 and C357 Al–Si-Mg alloys, the following conclusions may be drawn.

1. The weight of dross increases with increase in the holding period of the molten metal at temperatures in the range $735 \pm 5\,^{\circ}C$. The dross is always wet with the molten metal. Spinel is the main inclusion to form. Its amount is enhanced by the increase in either the Mg content, i.e., C357 alloy, or holding time, about 72 h. Carbides, e.g., Al_4C_3, may also occur.

2. Oxides (films or clusters) are the most influential parameter in determining the filtration time when using the PoDFA technique. However, during sampling, it is rather difficult to separate the individual effects of inclusions and oxides on the filtration time, and even more so if the molten metal is disturbed or not properly skimmed.

3. Although the PoDFA technique is a powerful tool in determining not only the inclusion densities but also the inclusions, the process is fairly long. Thus, an in-line measuring apparatus, e.g., Limca, may be recommended, especially in the preparation of critical components for aeronautical applications.

Appendix A

Details of chemical analysis and codes used for C357 alloy are given in Tables AI–AIII.

TABLE BIII Concentrations of major inclusions in C357 alloy

Experiment number	TiB_2 and TiC ($mm^2\ kg^{-1}$)	Al_4C_3 ($\leq 3\ \mu m$) ($mm^2\ kg^{-1}$)	Al_4C_3 ($> 3\ \mu m$) ($mm^2\ kg^{-1}$)	MgO ($mm^2\ kg^{-1}$)	MgO (cuboids) ($mm^2\ kg^{-1}$)	$MgAl_2O_4$ ($mm^2\ kg^{-1}$)
24D	—	0.0362	0.0904		0.009	0.3165
24E	—	0.028	0.0364	0.0028	0.0028	0.2103
24H	—	0.0822	0.2054	—	—	0.5341
25A	—	—	—	0.0668	0.0891	0.2896
25D	—	0.0987	0.3207	0.0493	0.0099	0.0148
25E	—	0.126	0.6302	0.0588	—	0.0252
25G	—	0.3877	0.7754	0.0646	0.0388	0.0258
26A	—	—	0.0364	0.4007	—	0.2914
26C	—	0.308	0.077	0.2695	—	0.1155
26D	10.4078	0.1156	0.1156	0.5782	—	0.3469
26E	3.6608	0.3405	0.0851	0.0851	—	0.0851
26H	7.6461	0.0831	0.1662	0.2493	—	0.1662
27B	7.7561	—	0.1724	—	—	0.6894
27C	9.824	0.117	0.3509	0.117	0.2339	1.0526
27D	10.4919	0.1206	0.1206	0.1206	0.2412	0.9648
28A	0.0568	0.0284	0.0094	0.0189	0.0948	0.7395
28D	0.1816	1.1354	0.0454	0.0227	0.1589	0.7266
29A	0.0215	0.5392	1.0785	—	0.1509	0.3451
29B	0.0231	0.4859	1.1338	—	0.2082	0.4396
29C	0.0259	0.5184	0.8814	0.1036	0.311	0.7258
29D	0.0221	0.3081	0.2208	0.0773	0.1656	0.3091
29E	0.0149	0.238	0.2975	0.1488	0.2231	0.5053
29F	0.015	0.4565	0.2518	0.2991	0.1417	0.4092
29H	0.0195	0.5472	0.254	0.3517	0.1954	0.5862
29I	9.1916	0.766	0.2553	1.2766	0.383	0.766

TABLE BIV Evaluation of Al_2O_3 films in C357 alloy

Experiment	Thin film			Thick film		
	Slight	Moderate	Heavy	Slight	Moderate	Heavy
24B			X			X
24D		X			X	
24E			X			X
24H		X			X	
25A	X			X		
25D	X			X		
25E	X			X		
25G	X			X		
26A			X			X
26C	X			X		
26D	X			X		
26E	X			X		
26H	X			X		
27B	X			X		
27C	X			X		
27D	X				X	
29D		X			X	
29E		X			X	
29F		X			X	
29H		X			X	
29I		X			X	

Appendix B

Details of the measured inclusions, oxide films and other parameters related to the alloy are presented in Tables BI–BIV.

Acknowledgements

The financial and other support received from the Natural Sciences and Engineering Research Council of Canada, the Centre Québécois de recherche et de développement de l'aluminium (Chicoutimi, Québec, Canada), Alcan Smelters and Chemicals Ltd (Jonquière, Québec, Canada), Bomem, Inc. (Québec City, Québec, Canada), Cercast Group (Montreal, Québec, Canada), Grenville Castings Ltd (Merrickville, Ontario, Canada), General Motors Powertrain Group (Saginaw, MI, USA), KB, Alloys, Inc. (Robards, KY, USA), Hi-Tech Ceramics, Inc. (New York, USA), Nemak–Alfa Industrial Group (Monterrey, Mexico) is gratefully acknowledged.

References

1. C. J. SIMENSEN and G. BERG, *Aluminium* **56** (1980) 335.
2. C. J. SIMENSEN, *Metall. Trans. B* **12** (1981) 733.
3. *Idem.*, PhD thesis, *Nor. Tek. Hoegsk.* (NTH), Trondheim, Norway (1982).
4. R. B. BLACKBURN, *Aluminium* **56** (1980) 585.
5. G. B. LE CONTE and K. BUXMANN, *ibid.* **55** (1979) 329.
6. C. J. SIMENSEN and U. HARTVEDT, *Z. Metallkde* **76** (1985) 409.
7. D. APELIAN and R. MUTHARASAN, *J. Metals* **32** (1980) 14.
8. W. SIMMONS and J. HACK, *Brit. Foundryman* **76** (1983) 10.
9. W. SIMMONS, *Foundry Trade J.* **158** (1985) 23.
10. W. SIMMONS and M. L. H. WISE, *Foundry Practice*, (1986) 217.
11. C. TIAN, PhD thesis, McGill Univeristy, Montreal, Québec (1994).
12. C. TIAN and R. I. L. GUTHRIE, in Proceedings of the International Symposium on Recent Developments in Light Metals, edited by M. Gilbert, P. Tremblay and E. Ozberk (The Metallurgical Society of The Canadian Institute of Mining, Metallurgy and Petroleum, Montreal, 1994) 415.
13. *Idem.*, *Light Metals* (1995) 1263.
14. G. DUBÉ and V. NEWBERRY, *ibid* (1983) 991.
15. C. CELIK and D. DOUTRE, *ibid* (1989) 793.
16. G. BÉLAND, C. DUPUIS and J.-P. MARTIN, *ibid.* (1995) 1189.
17. G. K. SIGWORTH and T. A. ENGH, *Metall. Trans. B* **13** (1982) 447.
18. P. WAITE and D. BERNARD, *Light Metals* (1990) 775.
19. J.-P. MARTIN and F. PAINCHAUD, *ibid* (1994) p. 915.
20. D. DOUTRE, B. GARIÉPY, J.-P. MARTIN and G. DUBÉ, *Light Metals* (1985) 1179.
21. S. A. LEVY, *ibid.* (1981) 773.
22. L. LIU and F. H. SAMUEL, *J. Mater. Sci.* (1997).
23. D. V. RAGONE, C. M. ADAMS and H. F. TAYLOR, *Amer. Foundrymens' Soc. Trans.* **64** (1953) 653.
24. M. C. FLEMINGS, F. R. MOLLARD, E. F. NIIYAMA and F. H. TAYLOR, *ibid.* **70** (1962) 1029.
25. S. F. LIU, M. G. FLEMINGS and F. H. TAYLOR, *Brit. Foundryman*, **53** (1960) 413.
26. S. VENKATESWARAN, R. M. MALLYA and M. R. SESHADRI, *Amer. Foundrymens' Soc. Trans.* **94** (1986) 701.

Received 24 March
and accpted 1 May 1997